Epipolar rectification of a generic camera

Marc Pierrot Deseilligny, Ewelina Rupnik

Published in Image Processing On Line on YYYY–MM–DD.
Submitted on YYYY–MM–DD, accepted on YYYY–MM–DD.
ISSN 2105–1232 © YYYY IPOL & the authors CC–BY–NC–SA
This article is available online with supplementary materials,
software, datasets and online demo at
https://doi.org/10.5201/ipol

Epipolar rectification of a generic camera

Marc Pierrot Deseilligny[1], Ewelina Rupnik[1]

[1] LASTIG, Univ Gustave Eiffel, ENSG, IGN, F-94160 Saint-Mande, France
(marc.pierrot-deseilligny@ensg.eu, ewelina.rupnik@ign.fr)

PREPRINT September 14, 2020

Abstract

ble

Keywords: epipolar rectification, generic camera, pushbroom sensor, central perspective

TODO :

1. dcrire mthode de calcul automatique des directions dans le cas sans modle;
2. Allgation : marche aussi sans modle, minimise globalement le critre d'erreur, formulation thorique de l'ambiguit et des condition d'existence d'un crire pipolaire; mesure de "l'pipolarabilit" d'un couple;

1 Introduction

The epipolar geometry of images plays a central role in many applications in the field of photogrammetry and computer vision. In the stereo-reconstruction pipeline, it is used twice:

1. In the camera pose orientation step, when computing the relative orientation of a pair of images from their corresponding points. Assuming the projection follows the central perspective and the internal calibration is known, one can compute the epipolar geometry of the images using the essential matrix. Finally, the relative orientation is recovered [**?**].
2. In the image dense matching step, where the epipolar rectification simplifies the correspondence search because for any point (x_1, y) in image I_1, its correspondence is some point (x_2, y) in image I_2. Therefore, finding correspondences across images reduces to a 1-dimensional problem (1D).

In this paper, we only study the epipolar rectification problem and more specifically its application to a generic camera model.

1.1 Related works

Rectifying a central perspective camera stereo pair involves transforming their original epipolar geometry to a canonical form where: (a) their focal planes are coplanar, and (b) their conjugate epipolar lines are colinear, and parallel to the camera's x-axis. From the algebraic standpoint, this is equivalent to applying two 2-dimensional (2D) projective transformations to both images of the stereo pair. Several approaches to computing such transformations have been proposed over the course of the last 30 years.

For a calibrated stereo pair (i.e. with known camera projection matrices), there exists a unique rectifying transformation, up to a rotation along the baseline [**?**]. In an uncalibrated case, the solution is obtained by factoring out two 2D homographies from the fundamental matrix. Because there are no two unique homographies, the common practice is to parametrize these transformations such that the distortions caused by the rectification process are minimized. For instance, Loop and Zhang [**?**] decompose the rectifying homographies to a combination of the projective, similarity and shearing transforms, with the condition that the prrojective transform remains (close to) affine. Hartley [**?**] satisfies the condition that for a neighborhood of a point (e.g. the center of an image), the computed homography is a rigid transformation. Building on this work, Isgro and Trucco's [**?**] approach obtains a unique solution by minimizing the x-disparity without having to explicitly calculate the fundamental matrix. Instead of minimizing the disparity in the first coordinate, Wu and Yu [**?**] recycle an idea first introduced by Hartley [**?**] which requires that the aspect ratio of the images before and after rectification is constant. More recently, Fusiello and Irsara [**?**] introduced the camera matrices back into the equation and proposed a *quasi*-Euclidean approach for uncalibrated cameras, similar to that of the calibrated cameras case. Their projective transformations are parametrized by five angles and a focal length. Monasse *et al.* [**?**] break down the one-time rotation of [**?**] to a three step procedure, and prove increased robustness by using a geometric error measure (i.e., camera rotation angle) to reduce the rectifying error distortions.

Unlike the central projection camera model, pushbroom-like sensors acquire each image row from a different perspective center. As a consequence, the epipolar lines are neither straight lines, nor are they conjugate across the image [**?**]. One way to overcome this particularity is to simplify the projection function with a 2D affine [**?**, **?**] or a parallel projection model [**?**]. Such approximations usually come at the price of precision, especially with the increasing camera field-of-view or in mountainous scenes. By extending the 2D affine model with two quaratic terms, Okamonoto *et al.* [**?**] demonstrates improved performance on SPOT images. In the context of dense image matching, de Francis *et al.* [**?**] improves the precision by partitioning the images into small patches, for which indepedent affine rectifictions are computed. Alternatively, and with equally good precision, Oh [**?**] uses the *Rational Polynomial Coefficients* (RPCs) to map the epipolar curves across the full size images with lines, in a piecewise approach, followed by a global rectification transformation using a polynomial function of 3^{rd} order.

1.2 Contributions

Our research work proposes an epipolar geometry rectification method that is not tied to any camera physical model. We demonstrate that on a range of models, including Pleiades images (pushbroom), the Corona images (panoramic pushbroom), a consumer grade camera images (central perspective) as well as Sentinel-1 radar images (pushbroom). The method resembles Oh's [**?**] approach in that it exploits the point correspondences to find the polynomial mapping to epipolar geometry. However, unlike the work of Oh [**?**], we do not require that the camera geometric model is known. We demonstrate that in some circumstances, point correspondences obtained from an image processing routine, e.g. SIFT [**?**], can serve to find the epipolar resampling.

In the remainder of this publication, we first outlay the mathematical background of the epipolar geometry and identify cases when epipolar geometry does not exist or is ambiguous (Section 2). Then, we introduce our method (Section 3), and finally present the experiments on different datasets with and without the geometric model (Section 4). The results are compared against the Oh's [**?**] method with respect to the y-parallax remaining after the resampling to the epipolar geometry.

2 The mathematics of epipolar geometry in the generic case

2.1 Formalisation and notation of projections

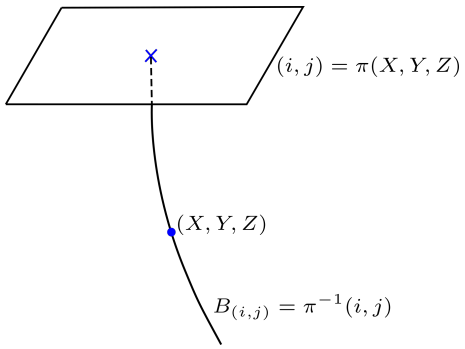

Figure 1: A projection and a bundle.

We define the geometric sensor model of an image by a projection function π, that computes, for a given 3D point, its 2D projection in the image:

Definition 1 (Generic geometric sensor model)**.** Illustrated in Figure 1.
A geometric sensor model π is a $\mathcal{C}^\infty$ mapping from ground space $(\mathbb{R}^3)$ to image space $(\mathbb{R}^2)$:

$$\pi : \mathbb{R}^3 \to \mathbb{R}^2, (X,Y,Z) \to (i,j) = \pi(X,Y,Z). \tag{1}$$

Next, we define the bundles of a projection:

Definition 2 (Bundle)**.** *For $p_k \in I_k$ we note $\mathcal{B}_k(p_k)$ the bundle corresponding to $\pi_k^{-1}(p_k)$. When there is no ambiguity, we note identically $\mathcal{B}_k(P)$, where $P \in \mathbb{R}^3$, the bundle corresponding to $\pi_k^{-1}(\pi_k(P)) = \mathcal{B}_k(\pi_k(P))$.*

Later, for simplicity, we will use the quasi-vertical hypothesis, which allows us to extend π to a bijective mapping of $\mathbb{R}^3$ and compute its inverse.

Definition 3 (Quasi-vertical camera model)**.** *We say that the projection is quasi-vertical if the following mapping $\widetilde{\pi}$ is a diffeomophism of $\mathbb{R}^3$:*

$$\widetilde{\pi} : \mathbb{R}^3 \to \mathbb{R}^3, (X,Y,Z) \to (i,j,Z) = \widetilde{\pi}(X,Y,Z), with (i,j) = \pi(X,Y,Z). \tag{2}$$

Given 2 images I_1 and I_2, the knowledge of their geometric models π_1 and π_2 reduces the matching between 2 images to a 1D problem. In fact, given a point p_1 in I_1, we can compute the 3D curve $\mathcal{B}_1(p_1)$ of ground points that project to p_1 in I_1, and compute its homologous curve in I_2 with $\pi_2(\mathcal{B}_1(p_1))$. We now define the H-compatible relation between two points by the following definition:

Definition 4 (H-Compatible, $\overset{\Longleftrightarrow}{\pi_1,\pi_2}$)**.** Illustrated in Figure 2.

We say that p_1 in I_1 and p_2 in I_2 are $\pi_1 - \pi_2$ H-compatible, and write $p_1 \overset{\Longleftrightarrow}{\pi_1,\pi_2} p_2$, if the following condition is satisfied:

$$(\mathcal{B}_1(p_1) \cap \mathcal{B}_2(p_2) \neq \emptyset) \Leftrightarrow (\exists P \in \mathbb{R}^3 : \pi_1(P) = p_1, \pi_2(P) = p_2). \tag{3}$$

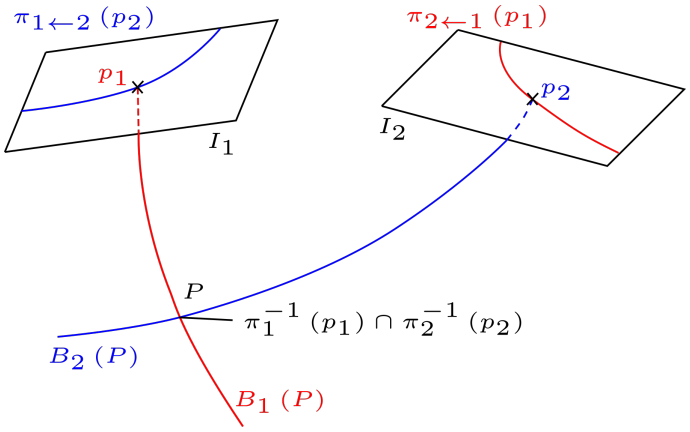

Figure 2: Illustration of $\overset{\Longleftrightarrow}{\pi_1,\pi_2}$

In image matching, the relationship $p_1 \overset{\Longleftrightarrow}{\pi_1,\pi_2} p_2$ means that p_1 and p_2 are potentially homologous.

2.2 Definition of the epipolar geometry

In fact, the previous relationships are sufficient to implement all the matching techniques and (π_1, π_2) can be used to define a matching process, taking advantage of the *a priori* knowledge of the scene geometry. That is, given a point in one image, we can easily follow its curve of potentially homologous points in the other image. This technique, which does not exploit the epipolar geometry, has the advantage of also being adaptable to multi-image matching. Epipolar geometry is therefore not strictly required for the image matching process.

The drawback of this approach is that it combines two different problems in the same procedure: the handling of the geometry and resampling and the matching process. When one is interested in the matching of a single image pair, the epipolar geometry can provide an elegant solution by separating the problem in two independent ones.

Definition 5 (Epipolar Geometry)**.** Illustrated in Figures 3 and 6.

Let π_1, π_2 be two cameras and let ϕ_1, ϕ_2 be two diffeomorphisms of $\mathbb{R}^2$. We say that ϕ_1, ϕ_2 are epipolar resamplings iff:

$$\forall e_1 = (u_1, v_1), e_2 = (u_2, v_2) : (v_1 = v_2) \Leftrightarrow (\phi_1^{-1}(e_1) \overset{\Longleftrightarrow}{\pi_1,\pi_2} \phi_2^{-1}(e_2)). \tag{4}$$

The matching of epipolar images is simplified because we know that the lines in two images are globally homologous.

Notation 1 (Epipolar line and curve.)**.** *We denote $\mathcal{L}_k(v)$ as the epipolar line of E_k defined by $v_k = v$. We also denote $\mathcal{C}_k(v)$ as the epipolar curve of I_k defined by $\mathcal{C}_k(v) = \phi_k^{-1}(\mathcal{L}_k(v))$*

We can see that when epipolar geometry exists, the two curves $\mathcal{C}_1(v)$ and $\mathcal{C}_2(v)$ are globally homologous:

$$\mathcal{C}_1(v) = \pi_1(\pi_2^{-1}(C_2(v))); \mathcal{C}_2(v) = \pi_2(\pi_1^{-1}(C_1(v))). \tag{5}$$

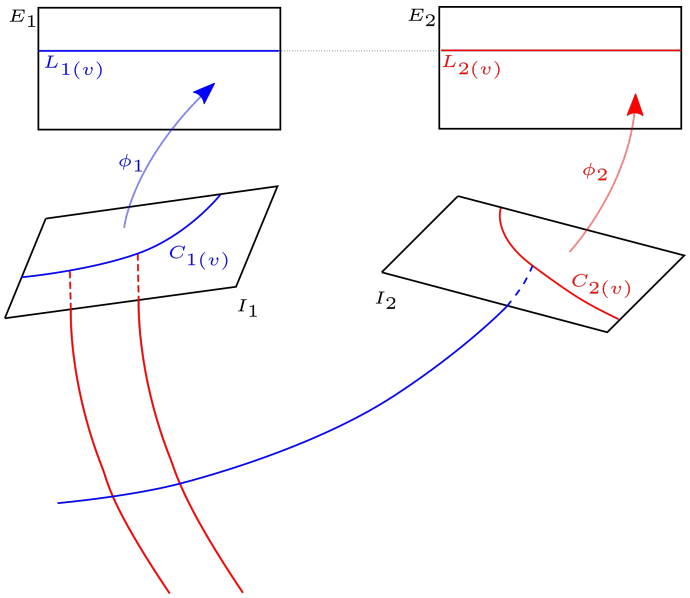

Figure 3: Illustration of epipolar geometry.

2.3 Existence of the epipolar geometry

We now discuss the existence of the epipolar geometry. As you will see, the epipolar geometry generally does not exist, and when it does, it is not unique. It is well known that:

- for any image pair following the central projection, there exists an epipolar geometry;
- not all image pairs can be resampled to epipolar geometry. For example, a cylindrical projection, applicable to many push-broom satellites, generally does not allow for epipolar resampling.

We explain now why the epipolar geometry does not exist for any π_1, π_2 and is instead an exception. Let's define the surface $\mathcal{S}_v^k$ of $\mathbb{R}^3$ by:

$$\mathcal{S}_v^k = \pi_k^{-1}(\mathcal{C}_k(v)). \tag{6}$$

By the definition of epipolar geometry above, it can be seen that $\mathcal{S}_v^1$ and $\mathcal{S}_v^2$ are the same surface $\mathcal{S}_v$:

$$\mathcal{S}_v^1 = \mathcal{S}_v^2 = \mathcal{S}_v. \tag{7}$$

For any $P \in \mathcal{S}_v^1$, set $e_1 = \phi_1(\pi_1(P)) = (u_1, v)$ and $e_2 = \phi_2(\pi_2(P)) = (u_2, v_2)$. We then have $\pi_1(P) \overset{\Longleftrightarrow}{\pi_1,\pi_2} \pi_2(P)$ because they are projections of the same point. Then, $v_2 = v$ according to Definition 5 and $P \in \mathcal{S}_v^2$. Furthermore, the $\mathcal{S}_v$ defines a foliation of $\mathbb{R}^3$, and it can be seen that:

$$\forall v \forall P \in \mathcal{S}_v : \mathcal{B}_1(P) \subset \mathcal{S}_v, \mathcal{B}_2 \subset \mathcal{S}_v, \tag{8}$$

which also leads directly from the definitions above. If $P \in \mathcal{S}_v$ then $\pi_k^{-1}(P) \in \mathcal{C}_k(v)$ (see equation (6)), then $\pi_k^{-1}(\pi_k(P)) = \mathcal{B}_k(P) \subset \mathcal{S}_v$. However, in general, the existence of a stable foliation for the two bundle sets, as expressed in Equation (8), cannot be satisfied, as illustrated in Figure 4. To explain further, let π_1 and π_2 be any two projections and suppose there exists a foliation satisfying the Equation (8). Then, let:

- P be any point in 3D space, and $\mathcal{S}_v$ be the surface such that $P \in \mathcal{S}_v$;
- $P_1 \neq P$ be a point on $\mathcal{B}_1(P)$, $P_1 \in \mathcal{S}_v$, then $\mathcal{B}_2(P_1) \subset \mathcal{S}_v$;

- $P_2 \neq P$ be a point on $\mathcal{B}_2(P)$, $P_2 \in S_v$, then $\mathcal{B}_1(P_2) \subset \mathcal{S}_v$.

As $\mathcal{B}_2(P_1)$ and $\mathcal{B}_1(P_1)$ are included in the same surface $\mathcal{S}_v$, they must intersect somewhere in a point Q. In the general case, the above is a contradiction because there is no reason that the condition $\mathcal{B}_2(P_1) \cap \mathcal{B}_1(P_2) \neq \emptyset$ is satisfied for any two sets of bundles (see Figure 4,right).

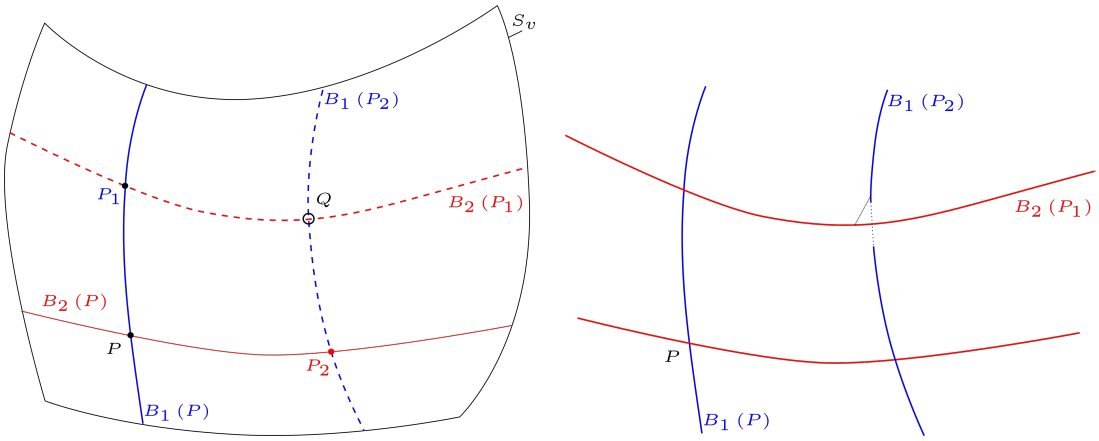

Figure 4: Path closure. Left: in the epipolar case, the bundles are on the same level of the foliation and the intersection. Right: in the generic case, the paths don't intersect and no epipolar geometry exists.

2.4 A local characterization of the epipolar existence

In this section, we compute a local formula (i.e. a differential equation) that provides conditions for the existence of an epipolar geometry. This section is rather theoretical and can be omitted by readers mainly interested in practical applications.

Analogously to the proof in Section 2.3, we will make a computation of two-way paths, $\mathcal{B}_1$ then $\mathcal{B}_2$, as well as $\mathcal{B}_2$ then $\mathcal{B}_1$. Then, we express the Taylor expansion of the intersection distance between these two paths . Let's consider the following (see Figure 5):

- we make the quasi-vertical assumption (note that we could use curvilinear abscissa when this assumption can not be satisfied);

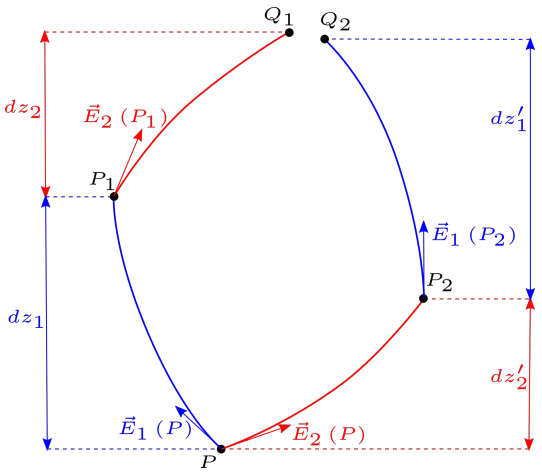

Figure 5: Notation for local characterization of the epipolar existence

- let P be any point in $\mathbb{R}^3$;
- consider the first path (P, P_1, Q_1) following $\mathcal{B}_1$ then $\mathcal{B}_2$, making a progression d_{z_1} on $\mathcal{B}_1$ and d_{z_2} on $\mathcal{B}_2$;
- consider a second path (P, P_2, Q_2) following $\mathcal{B}_2$ then $\mathcal{B}_1$, making a progression $d_{z_2'}$ on $\mathcal{B}_1$ and $d_{z_1'}$ on $\mathcal{B}_2$;
- we denote $\overrightarrow{t_1(P)} = (x, y, 1)$ as the tangent to the bundle $\mathcal{B}_1$ in point P (and similarly $\overrightarrow{t_2}(P)$);
- when we write $\frac{\partial F}{\partial z_1}$, we will refer to the coordinate system $(i_1, j_1, z) = \widetilde{\pi}_1^{-1}(x, y, z)$, idem for $\frac{\partial F}{\partial z_2}$, and obviously as they are two different coordinate systems, we have in general $\frac{\partial F}{\partial z_1} \neq \frac{\partial F}{\partial z_2}$.

Now, for any pair of "small" values (δ_1, δ_2), we compute (δ_1', δ_2') which minimize the distance $|Q_1, Q_2|$ and express the canceling of the second degree Taylor expansion of this distance (the first degree can always be canceled out as we will see). Noting δ the max of all δ, the second degree Taylor expansion gives :

$$P_1 = P + \delta_1 \overrightarrow{t_1(P)} + \frac{{\delta_1}^2}{2} \frac{\partial \overrightarrow{t_1}}{\partial z_1}(P) + \mathcal{O}(\delta^3) \tag{9}$$

$$Q_1 = P_1 + \delta_2 \overrightarrow{t_2(P_1)} + \frac{{\delta_2}^2}{2} \frac{\partial \overrightarrow{t_2}}{\partial z_2}(P_1) + \mathcal{O}(\delta^3) \tag{10}$$

$$\overrightarrow{t_2(P_1)} = \overrightarrow{t_2(P)} + \delta_1 \frac{\partial \overrightarrow{t_2}}{\partial z_1}(P) + \mathcal{O}(\delta^2) \tag{11}$$

Putting together Equations (9), (10), (11) we can perform a Taylor expansion of the path P to Q_1:

$$Q_1 = P + \delta_1 \overrightarrow{t_1(P)} + \delta_2 \overrightarrow{t_2(P)} + \frac{{\delta_1}^2}{2} \frac{\partial \overrightarrow{t_1}}{\partial z_1}(P) + \frac{{\delta_2}^2}{2} \frac{\partial \overrightarrow{t_2}}{\partial z_2}(P) + \delta_1 \delta_2 \frac{\partial \overrightarrow{t_2}}{\partial z_1}(P) + \mathcal{O}(\delta^3) \tag{12}$$

And similarly for P to Q_2 :

$$Q_2 = P + \delta_2' \overrightarrow{t_2(P)} + \delta_1' \overrightarrow{t_1(P)} + \frac{{\delta_2'}^2}{2} \frac{\partial \overrightarrow{t_2}}{\partial z_2}(P) + \frac{{\delta_1'}^2}{2} \frac{\partial \overrightarrow{t_1}}{\partial z_1}(P) + \delta_1' \delta_2' \frac{\partial \overrightarrow{t_1}}{\partial z_2}(P) + \mathcal{O}(\delta^3) \tag{13}$$

The first degree Taylor expansion of $Q_2 - Q_1$ gives :

$$Q_2 - Q_1 = (\delta_1' - \delta_1) \overrightarrow{t_1(P)} + (\delta_2' - \delta_2) \overrightarrow{t_2(P)} + \mathcal{O}(\delta^2) \tag{14}$$

To minimize $|Q_2 - Q_1|$, the first step is to cancel the first degree terms of $Q_2 - Q_1$. We assume that $\overrightarrow{t_2(P)}$ and $\overrightarrow{t_1(P)}$ are independant vectors[1] and we must then make $\delta_2' - \delta_2$ and $\delta_1' - \delta_1$ second degree terms:

$$\Delta_1 = \delta_1' - \delta_1 = \mathcal{O}(\delta^2) \ ; \ \Delta_2 = \delta_2' - \delta_2 = \mathcal{O}(\delta^2) \tag{15}$$

To develop $Q_2 - Q_1$ we can use the following identities that are direct consequences of Equation (15):

$$\delta_1 \delta_2 - \delta_1' \delta_2' = \mathcal{O}(\delta^3) \ ; \ {\delta_1}^2 - {\delta_1'}^2 = \mathcal{O}(\delta^3) \ ; \ {\delta_2}^2 - {\delta_2'}^2 = \mathcal{O}(\delta^3) \tag{16}$$

[1] Otherwise, it would be a degenerate case for stereovision

Subtracting Equation (12) from Equation (13), and using Equation (16), we can write :

$$Q_2 - Q_1 = \Delta_1 \overrightarrow{t_1(P)} + \Delta_2 \overrightarrow{t_2(P)} + \delta_1\delta_2(\frac{\partial \overrightarrow{t_2}}{\partial z_1}(P) - \frac{\partial \overrightarrow{t_1}}{\partial z_2}(P)) + \mathcal{O}(\delta^3) \tag{17}$$

We now translate the intersection of paths by canceling the second degree Taylor expansion in $Q_2 - Q_1$. We have three vectors, and their weighted sum can be null iff they are colinear.

Theorem 1 (Existence of epipolar)**.** *The epipolar geometry exists iff the following determinant is null:*

$$\left[\begin{array}{c|c|c} \overrightarrow{t_1} & \overrightarrow{t_2} & \frac{\partial \overrightarrow{t_2}}{\partial z_1} - \frac{\partial \overrightarrow{t_1}}{\partial z_2} \end{array} \right] = 0 \tag{18}$$

Remark 1 (Epipolar equation with central perspective camera)**.** *As an illustration in an easy case, we can see that this condition is trivially satisfied for a pair of central perspective cameras as we have the canceling of both terms as shown in Equation (19). This is because for a given point P, for any point P_1 on $\mathcal{B}_1(P)$, $\overrightarrow{t_2P_1}$ belongs to the epipolar plane $\mathcal{P}$. We have $\overrightarrow{t_2P_1} \in \mathcal{P}$, so $\frac{\partial \overrightarrow{t_2}}{\partial z_1} \in \mathcal{P}$, and as we have also $\overrightarrow{t_1(P)} \in \mathcal{P}, \overrightarrow{t_2(P)} \in \mathcal{P}$, the collinearity between $\overrightarrow{t_1(P)}$, $\overrightarrow{t_2(P)}$ and $\frac{\partial \overrightarrow{t_2}}{\partial z_1}(P)$ is thus proven.*

$$\left[\begin{array}{c|c|c} \overrightarrow{t_1} & \overrightarrow{t_2} & \frac{\partial \overrightarrow{t_2}}{\partial z_1} \end{array} \right] = \left[\begin{array}{c|c|c} \overrightarrow{t_1} & \overrightarrow{t_2} & \frac{\partial \overrightarrow{t_1}}{\partial z_2} \end{array} \right] = 0 \tag{19}$$

2.5 Ambiguity of the epipolar geometry

When the epipolar geometry exists, the epipolar resampling is not unique. To demonstrate that our rectification method handles this ambiguity rigorously, we first describe it formally.

Let ϕ_1, ϕ_2 and ϕ'_1, ϕ'_2 be two epipolar resamplings, then, for any v consider the pair of lines $\mathcal{L}_1(v), \mathcal{L}_2(v)$:

- $\phi_k^{-1}(\mathcal{L}_k(v))$ is the curve $\mathcal{C}_k(v)$ by definition of epipolar resampling;
- and $\phi'_k(\mathcal{C}_k(v) = \phi'_k(\phi_k^{-1}(\mathcal{L}_k(v)))$ is a line, also by definition of epipolar resampling;
- and still by definition $\phi'_1(\phi_1^{-1}(\mathcal{L}_1(v))) = \phi'_2(\phi_2^{-1}(\mathcal{L}_2(v)))$;

Consequently we have the following constraint between two pairs of epipolar ressampling:

- $\phi'_1\phi_1^{-1}$ and $\phi'_2\phi_2^{-1}$ are diffeomorphisms transforming lines into lines;
- $\phi'_1\phi_1^{-1}$ and $\phi'_2\phi_2^{-1}$ define the same global transformation on lines (i.e. if $\phi'_1(\phi_1^{-1}(\mathcal{L}_1(v))) = \phi'_2(i\phi_2^{-1}(\mathcal{L}_2(v))))$.

Vice versa, let ϕ_1, ϕ_2 be an epipolar resampling and let Λ_1, Λ_2 be diffeomorphisms that are stable for lines and make globally the same transformation on lines. We can thus note that $\Lambda_1 \circ \phi_1$ and $\Lambda_2 \circ \phi_2$ are also an epipolar resampling.

Having devised the exact ambiguity, we can now define two constraints to impose on a unique epipolar resampling:

1. Constraint on the uniqueness of the deformation inside each line . For instance, one can impose that the colums remain constant (i.e. the deformation is only made on y), as given in Equations (20) and (21);
2. Constraint on the global deformation of lines[2]. For instance, by fixing the transformation of one image, as given in Equation (6).

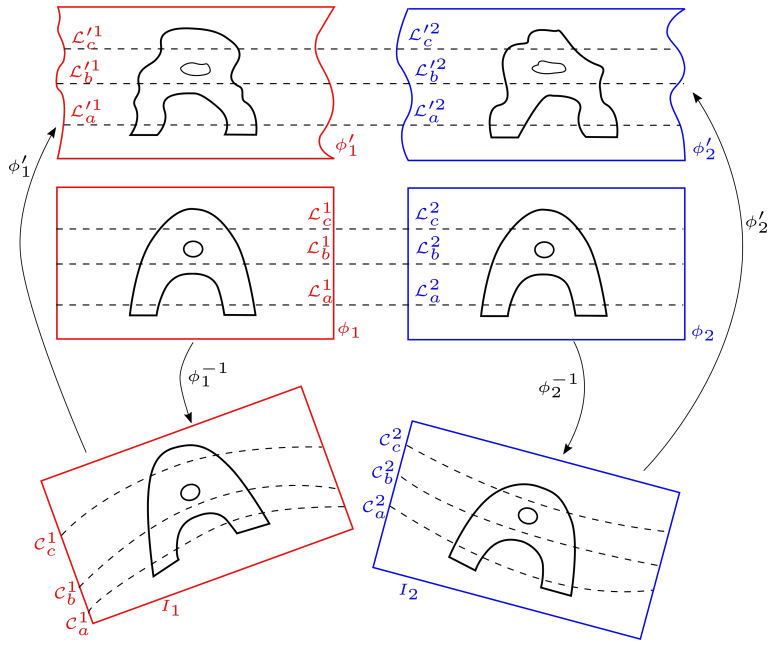

Figure 6: Ambiguity of the epipolar geometry: two possible epipolar resamplings for a single stereopair.

Theorem 2 (Unique epipolar constraint)**.** *If the epipolar geometry exists, there exists a unique epipolar resampling ϕ_1, ϕ_2 satisfying the following three constraints:*

$$\phi_1(x, y) = (x, y') \tag{20}$$

$$\phi_2(x, y) = (x, y') \tag{21}$$

$$\phi_1(0, y) = (0, y) \tag{22}$$

3 Proposed method for epipolar geometry resampling

3.1 Hypothesis and layout

3.1.1 Principles

The principle of the method is to use *H-Compatible* points p_1, p_2 to calculate a pair of functions ϕ_1, ϕ_2 that comply with the epipolar constraint, i.e. *"$\phi_1(p_1)$ and $\phi_2(p_2)$ are on the same line"*. As these epipolar functions are not unique, we parameterize the ϕ_k in Theorem 2 accordingly:

$$\phi_k(i, j) = (i, V_k(i, j)); \quad V_k : \mathbb{R}^2 \to \mathbb{R} \tag{23}$$

This parametrization implements the constraints of Equations (20) and (21). We will account for the constraint of Equation (22) in Section 3.2.1[3]. To compute V_1, V_2, for any pair of *H-Compatible*

[2] i.e. where each line is transformed globally to another line
[3] See Equations (29), (30).

Figure 7: Left: a set of epipolar lines not handled by our method. Right: a perfectly acceptable pair of epipolar lines.

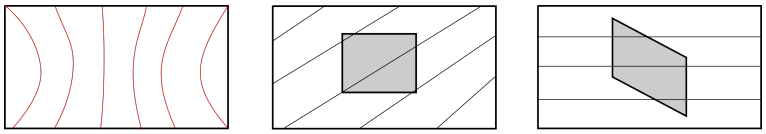

Figure 8: Left: quasi-vertical epipolar curve for which correction with Equation (23) is impossible. Middle and right: oblique curves for which epipolar rectification with Equation (23) is possible but generates significant distortion.

points, we add an observation that constrains V_1 and V_2:

$$V_1(p_1) = V_2(p_2). \tag{24}$$

3.1.2 Hypothesis

The method takes two camera models π_1 and π_2 as inputs. These models are considered black-boxes that satisfy Equation (1), and for which no specific assumption is made on the physical model of the camera. In our C++ implementation, the cameras are considered to be pure virtual classes offering the interface to Equation (1). In this paper, the examples processed by our method are pushbroom satellite models known by their RPCs, the central perspective and radar models. However, the only restriction imposed on the generic nature of the model is that the projection function is "smooth", i.e.:

- π are $\mathcal{C}^\infty$ functions, and
- the directions of epipolar curves vary within a limited range (for example, less than $\frac{\pi}{2}$).

Figure 7 illustrates the latter constraint. The left image presents a set of epipolar lines with too large direction variations. The right image represents a pair of epipolar lines whose directions change within a small range, therefore suitable for the proposed resampling method.

3.1.3 Estimation of the center and the global direction

To begin with, the method estimates the centers C_1, C_2 of a set of points p_1 and p_2. This is done by calculating the average of all points' coordinates. Then, the computations continue in the coordinate systems centered at C_1, C_2. After this "normalisation", the constraint in Equation 22 is applied at these centers.

BEGIN-BEGIN-BEGIN

Then we need to compute a coordinate system where epipolar lines are globaly horizontal. This requirement is a consequence of equation (23), and is illustrated by Figure 8:

- left image of figure 8 presents a case where epipolar curve are quasi vertical and for which an epipolar correction, without initial rotation, according to equation (23) would be impossible;

- middle image of figure 8 presents a case where epipolar curve are oblique, in this case epipolar correction according to equation (23) would be possible but would lead to important distorsion in the image, as can be seen on left image.

So for each image we estimate the average direction $\vec{D}_k$ of its epipolar lines, and using Equation (25), a rotation R_k is applied to the input point.

$$R_k(p) = \frac{p - C_k}{\vec{D}_k} \tag{25}$$

The epipolar lines are now globally horizontal and the subsequent epipolar deformation can be computed on the rotated data points.

END-END-END

3.1.4 Layout

The layout of the method follows three steps: (1) estimate the global direction of epipolar lines; (2) estimate F_1, F_2 as the local epipolar rectification in the coordinate system linked to the global direction; (3) estimate the final epipolar rectification as a composition of F_1, F_2 and the rotation. A more formalized description of the algorithm is given in Algorithm 1.

Algorithm 1 Epipolar(π_1,π_2). *Layout of the algorithm for computing the epipolar rectification from camera models*

Use π_1, π_2 to estimate a set of *H-Compatible* points $\mathcal{H} = \{(p_1, p_2)\}$:
Estimate centers C_1 and C_2;
Estimate global direction of epipolars $\vec{D}_1$ and $\vec{D}_2$,
Estimate rotations R_1, R_2 according to Equation (25)
for all $p_1, p_2 \in \mathcal{H}$ **do**
  set: $q_1 = R_1(p_1)$, $q_2 = R_2(p_2)$
  add equation: $V_1(q_1) = V_2(q_2)$
end for
estimate with the least squares method V_1 and V_2
set $F_k(x, y) = (x, V_k(x, y))$
set $\phi_k = F_k \circ R_k$
return (ϕ_1, ϕ_2)

3.1.5 Why does our method work?

Intuitively, it may not be obvious that the system of equations in Equation (24) is well posed. In fact, if there was a functional relationship between p_1 and p_2, as $p_1 = F(p_2)$, an infinity of solutions for (V_1, V_2) would exist, because for any function $V : \mathbb{R}^2 \to \mathbb{R}$ we can generate a solution $(V, V \circ F)$.

However, note that due to the 3D aspect of p_1 and p_2, there is *no* functional relationship between them and, consequently, there are more constraints on (V_1, V_2). Instead of a functional relationship, we can generate "one to many" (and "many to one") correspondences as illustrated in Figure 9. For example, for a given point p_1, following the curve $\pi_2(\mathcal{B}_1(p_1))$, we can generate several points on the bundle (potentially an infinity) which results in many correspondences. To illustrate, if we take p_2^k to be multiple homologous points of p_1, we then have the equation:

$$V_1(p_1) = V_2(p_2^1)\ ;\ V_1(p_1) = V_2(p_2^2)\ ;\ V_1(p_1) = V_2(p_2^3) \ldots, \tag{26}$$

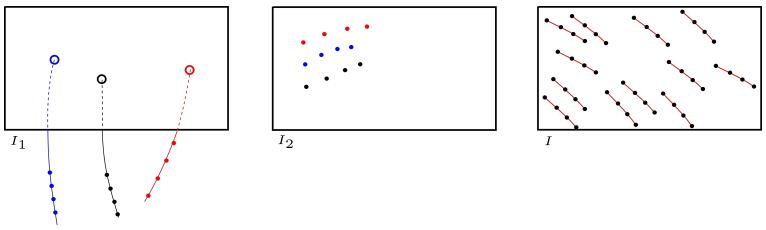

Figure 9: Left: for each p_1, we generate several 3D points on $B_1(p_1)$. Middle: the multiple correspondences in I_2. Right: a dense network of curves in I_2.

which in fact enforces this constraint:

$$V_2(p_2^1) = V_2(p_2^2) = V_2(p_2^3) \dots \tag{27}$$

If we now look at left image of Figure 9, we see that Equation (27) imposes the constraint that a "piece of curve" is horizontal. In Section 3.3.1, we will see a more detailed analysis explaining how the method can work even with configurations different than those depicted in Figure 9.

3.2 Detailed implementation

3.2.1 Choice of a parametric functional space

We need to select a space of parametric functions to represent V_1, V_2. The only constraint is that V_1, V_2 are $\mathcal{C}^\infty$ functions, and that the additional constraint in Equation (22) is valid.

Classically, when parameterizing a set of functions $\mathcal{C}^\infty$, a "natural" candidate is the set of polynomials of a given degree. We know that the function will be $\mathcal{C}^\infty$ and, according to the Stone-Weierstrass theorem [**?**, **?**] (which says that the space of polynomials is dense in the space of continuous functions), with a sufficiently high degree we will be able to accurately approximate any continuous function. A possible limitation of selecting high degree polynomial is over-fitting, which may lead to unwanted high frequency behavior. In our case, this problem should never arise as the measurements are synthesized from the projection functions π_1, π_2, which provides sufficient redundancy (for instance, hundreds of times more measurements than constraints). Note, this will be a different issue, and we will have to take care of degree, when we use the method with tie points and without model in section 3.3.1

If d is the selected degree, we have two vectors of unknowns $C^1_{a,b}, C^2_{a,b}$, corresponding to coefficients of the polynomials:

$$V_k(p) = V_k(i,j) = \sum_{a=0}^{d} \sum_{b=0}^{d-a} C^k_{a,b} i^a j^b. \tag{28}$$

3.2.2 Imposing constraints on global lines deformation

When applying the constraint of equation (22) to equation (28), we have $i = 0$, thence we can suppress all terms i^a for $a \neq 0$. The constraint equation then reads:

$$V_1(0,j) = j = \sum_{b=0}^{N} C^1_{0,b} j^b \tag{29}$$

In Equation (29), j on the left and the sum on the right are both polynomials, so if their functions are equal on a segment, they must be equal term by term. The constraint then comes to force a

number the unknowns $C^1_{0,k}$ which have known values: 1 for $C^1_{0,1}$ and 0 otherwise. Using the Kronecker delta, we can write:

$$C^1_{0,k} = \delta_{1,k} \tag{30}$$

3.2.3 Generation of points, computation of the direction and centers

The points from π_1 and π_2 are generated twice, using each image as the master. The bundles are always generated from the master images. The Algorithm 2 presents the generation of the points with I_1 as the master, as well as the computation of the global direction and the points' centers.

Algorithm 2 GenerateData(). *Compute a list $L_{1,2}$ of $\pi_1 - \pi_2$ H-compatible pairs with I_1 as the master image. Compute also the center C_1 of points in I_1 and the global direction $\vec{D}_2$ for epipolar curves of I_2.*

$L_{1,2} \leftarrow ()$; $C_1 \leftarrow (0,0)$; $\vec{D}_2 \leftarrow \overrightarrow{(0,0)}$; $N \leftarrow 0$
for $p_1.x = 0$ **to** X_1 **Step** $\delta_{x,y}$ **do**
  for $p_1.y = 0$ **to** Y_1 **Step** $\delta_{x,y}$ **do**
    for $z = Z_0$ **to** Z_1 **Step** δ_z **do**
      $p_2 = \pi_2(\widetilde{\pi}_1^{-1}(p_1, Z))$
      $p'_2 = \pi_2(\widetilde{\pi}_1^{-1}(p_1, Z + \delta_z))$
      if $p_2 \in I_2$ **and** $p'_2 \in I_2$ **then**
        $L_{1,2}.append((p_1, p_2))$
        $C_1 \leftarrow C_1 + p_1$
        $\vec{D}_2 \leftarrow \vec{D}_2 + \frac{\overrightarrow{p_2 p'_2}}{|p_2 p'_2|}$
        $N \leftarrow N + 1$
      end if
    end for
  end for
end for$C_1 \leftarrow \frac{C_1}{N}$; $\vec{D}_2 \leftarrow \frac{\vec{D}_2}{N}$

Once the centers C_1, C_2, directions $\vec{D}_1, \vec{D}_2$ and the list $L_{1,2}$ are computed, they are used to normalize the measurements and make the direction globally horizontal by applying Equation (25) to all elements of the list.

3.2.4 Estimating the rectification

As the measurements are synthetic and without outliers, we can directly solve the equations with the linear least squares method, thus merging all previous steps:

- let d be the degree of the polynomials;
- the unknowns are the coefficient of the polynomials V_1 and V_2. There are $\frac{(d+1)(d+2)}{2}$ unknowns for V_2 and $\frac{(d+1)(d+2)}{2} - (d+1)$ for V_1, taking into account the constraint in Equation (30);
- for each pair of normalized points q_1, q_2 we add the Equation (28) to the least squares equation system.

We then estimate the V_1, V_2 and obtain:

$$\varphi_k(p) = \varphi_k(i,j) = (i, V_k(i,j)) \; ; \; \phi_k = \varphi_k \circ R_k \tag{31}$$

Estimating the inverse function The natural way to resample I_k in E_k is to write:

$$E_k(p) = I_k(\phi_k^{-1}(p)). \tag{32}$$

Therefore, to rectify an image, we also need to calculate the inverse function. The inverse of R_k is obvious. For computing the inverse of φ_k, we exploit the fact that if φ is invariant for the column, then φ^{-1} is invariant too. Consequently, we can parametrize it with a function $W : \mathbb{R}^2 \to \mathbb{R}$ as:

$$\varphi_k^{-1}(p) = \varphi_k^{-1}(u, v) = (u, W_k(u, v)) \tag{33}$$

To estimate W, we follow the same rationale as in Section 3.2.1, and use the base of a polynomial function. Once the V_k are known, we generate for each point $p_k = (i, j)$ in $L_{1,2}$ an observation:

$$W_k(i, V_k(i, j)) = j \tag{34}$$

If we want to ensure that the computed inverse is sufficiently close to the "real" inverse, we can increase the polynomial's degree (in our implementation, we typically use the degree of $d + 4$). It has no side effects as long as we maintain high redundancy.

BEGIN-BEGIN-BEGIN

3.3 Epipolar resampling without the geometric model – not too happy with this section me neither (;-)

3.3.1 Possibility with only tie-points

Ideally, there is no bullet-ing but full sentences.

"Is it possible to use the proposed method to compute the epipolar geometry if we have point correspondences between the image pairs but we don't know the geometric model?" There is NO ~~a~~ straightforward answer to whether it is possible or not. The answer is that is not possible in general, but it becomes possible when the relief is not smooth and we add the contraint that the ressampling is smooth enough.

Pro: Algorithm 1 uses only point correspondences and a direction to compute the epipolar geometry. It does not matter if the point correspondences are extracted from the geometric model (as with Algorithm 2) or from an image processing method, e.g. SIFT [**?**], which does not require any *a priori* information on image geometry. Hence, as long as we know the directions, our method can be used.

Cons: When the point correspondences are computed with an image processing routine, there exists some functional relationship between them. Suppose that:

- the 3D scene can be described by a function $Z = \mathcal{Z}(X, Y)$, and denote $S^{\mathcal{Z}}$ as the corresponding surface;
- for a point p_1 of I_1, denote $\widetilde{\pi}_1^{\mathcal{Z}}(p_1)$ as the intersection of $\mathcal{B}_1(p_1)$ and the surface $S^{\mathcal{Z}}$; $\widetilde{\pi}_1^{\mathcal{Z}}$ is the inverse of the restriction π_1 as function from I_1 to $S^{\mathcal{Z}}$.

We now see that there exists a functional relationship between all the point correspondences (p_1, p_2) and it follows the equation:

$$p_2 = (\pi_2 \circ \widetilde{\pi}_1^{\mathcal{Z}})(p_1) = F^{\mathcal{Z}}(p_1). \tag{35}$$

Therefore, as discussed in Section 3.1.5, in the most general case, it is impossible to recover the epipolar geometry from a set of correspondences.

Pro & Cons: If we go back to Section 3.1.5, we can see that we missed the fact that in the proposed method, the functions V_1 and V_2 have to be "smooth". Let's reason again:

- suppose we have computed an epipolar geometry: $e_k = (u_k, v_k) = \phi_k(p_k) = (x_k, V_k(y_k)$, with $v_1 = v_2$ and V_k being a "smooth" function and we try to analyze if the geometry was ambiguous;
- we have $e_2 = (\phi_2 \circ \pi_2 \circ \widetilde{\pi}_1^{\mathcal{Z}} \circ \phi_1^{-1})(e_1) = P(e_1)$
- we write the previous equation as $(u_2, v_2) = P(u_1, v_1) = (u_1 + p_x(u_1, v_1), v_1)$, where p_x is what is usually called the "parallax function";
- as in Section 3.1.5, for any function $W_2 : \mathbb{R}^2 \to \mathbb{R}$, let W_1 be the function defined by $W_1 = W_2 \circ P$;
- then, for any e_1, e_2, $(u_1, W_1(u_1, v_1))$ and $(u_2, W_2(u_2, v_2))$, we also satisfy the epipolar constraint as $W_1(u_1, v_1)) = W_2(P(u_1, v_1)) = W_2(u_2, v_2)$.

Is it possible that W_2 and $W_2 \circ P$ are both smooth functions? This depends on the smoothness of P. If P is itself a smooth function, then obviously for any smooth W_2, $W_2 \circ P$ will also be smooth and the epipolar resampling will be ambiguous. If we take the canonical example of a flat 3D scene, then $p_x = 0$, $P = Id$ and as $W_1 = W_2$, W_1 is smooth if W_2 is smooth. In this case the epipolar geometry is also ambiguous. However, if the scene has high frequency depth changes, then P also has high frequencies, and W_2 and $W_2 \circ P$ cannot both be smooth. This can be seen more formally by the following equation:

$$\frac{\partial W_2 \circ P}{\partial u} = \frac{\partial P}{\partial u} \frac{\partial W_2}{\partial u} \circ P \tag{36}$$

As an archetype case, for any point where the scene is not differentiable, we have $\frac{\partial P}{\partial u} = \infty$ and Equation (36) which lead to $\frac{\partial W_2}{\partial u} = 0$ because $W_2 \circ P$ is supposed to be smooth. If W_2 is a polynom of limited degree, and we have sufficient number of points with, $\frac{\partial W_2}{\partial u} = 0$, then it will conduct to the fact that W_2 depends only of v, adding finally equation (22), we have the $W_2 = Id$, which show the uniqueness of the solution.

3.3.2 Estimating the directions without model

For using our methods, with tie-points, we need also a way to estimate the global directions, as it is done in section **??** when we have the geometric models.

In the implemantation we provide, we give two options to the user : provide it or let the programm compute it automatically. Obviously the providing option can be safer when the user has sufficient knowledge on the acquisition; it can be used for examle with like satellite along the track , like in the example we provide with Corona acquisition. The automatic option is based on a discretization of possible directions and combinatorial exploration of all the pair of possible direction ; for a given pair, a quality criterion is computed on residual of epipolar ressampling with degree 0 TO CHECK !!! , using a $L1$ norm (to be more robust to outliers).

Faut il donner un algorithme ? Ou est-ce suffisement simple pour tre potentiellement clair ? END-END-END

4 Experiments

Datasets:

- Corona, +MPD, les courbes (teorique fait par Benjamin)
- Pleiades, residu

	Oh [?]				Ours			
	B/H				B/H			
Z_{buff} [m]	0.1	0.15	0.25	0.45	0.1	0.15	0.25	0.45
50	0.0070	0.0142	0.0156	0.0084	0.0017	0.0017	0.0017	0.0012
100	0.0065	0.0144	0.0157	0.0092	0.0019	0.0018	0.0017	0.0012
200	0.0057	0.0151	0.0164	0.0098	0.0027	0.0022	0.0022	0.0014
270	0.0055	0.0156	0.0144	0.0010	0.0036	0.0026	0.0026	0.0020

Table 1: Maximum value of the remaining y-parallax [pix] for acquisitions from a **single orbit**. Z_{buff} corresponds to half the depth of the volumne used in the resampling calculation.

	Oh [?]				Ours			
	B/H				B/H			
Z_{buff} [m]	0.13	0.2	0.3	0.4	0.13	0.2	0.3	0.4
50	0.0297	0.0059	0.0178	0.0112	0.0021	0.0021	0.0021	0.0021
100	0.0284	0.0088	0.0183	0.0134	0.0029	0.0037	0.0034	0.0034
200	0.0325	0.0196	0.0252	0.0232	0.0064	0.0010	0.0086	0.0088
270	0.0381	0.0311	0.0343	0.0340	0.0101	0.0171	0.0143	0.0154

Table 2: Maximum value of the remaining y-parallax [pix] for acquisitions from **multiple orbits**. Z_{buff} corresponds to half the depth of the volumne used in the resampling calculation.

	Single orbit				Multiple orbits			
	B/H				B/H			
Z_{buff} [m]	0.1	0.15	0.25	0.45	0.13	0.2	0.3	0.4
50-270	$1.6e^{-5}$	$0.8e^{-5}$	$0.3e^{-5}$	$0.1e^{-5}$	$2.0e^{-5}$	$0.7e^{-5}$	$0.5e^{-5}$	$0.2e^{-5}$

Table 3: Epipolarability indices for acquisitions from a single and multiple orbits.

- Spot
- nous
- Oh

Exemple de rsultats avec rsidus. + qq crop d'images rectifiees.

4.1 Satellite images

C'est la que c'est vraiment utile ....

4.2 Radar images

?

4.3 Images without the geometric model

Corona KH-4B images Expos precis avec modele analytique:

* calcul des points homologues, en 3D =¿ direction moyenne * resolution par moindres carress avec degres lev, degr sup pour l'inverse * Utilit du 3D, precision en fonction de la nappes, possibilit d'utiliser un modle 3D grossier .

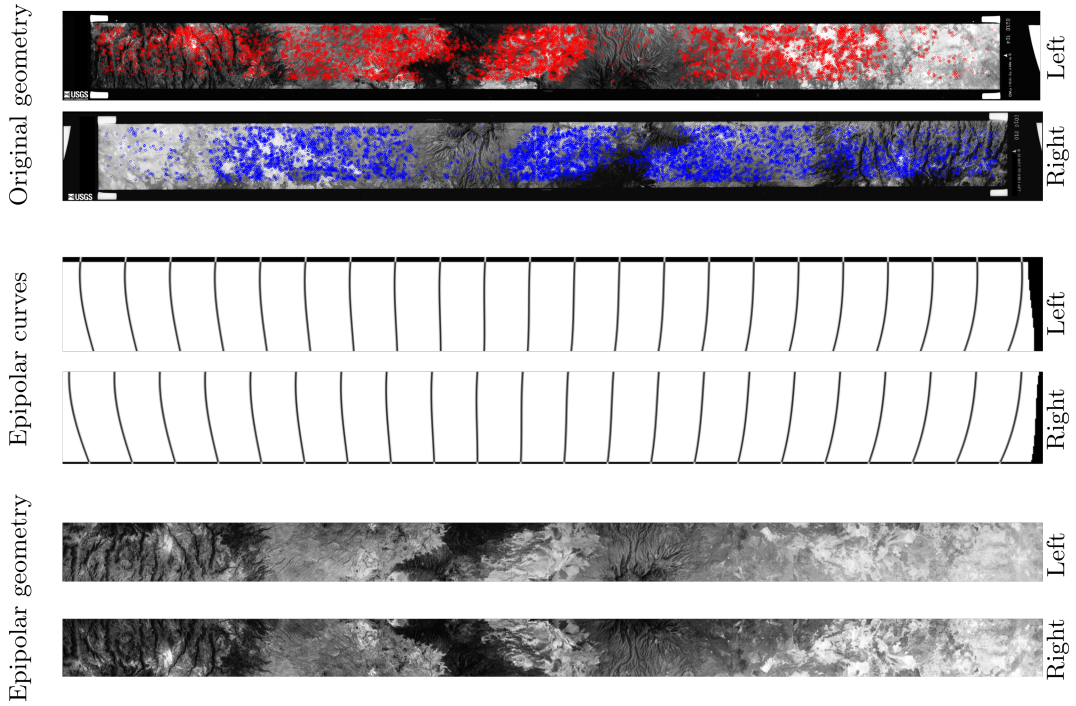

Figure 10: Corona KH-4B steropair and the point correspondences (top); the epipolar curves in the original geometry of the stereopair (middle); and the stereopair resampled to the epipolar geometry, rotated by 90° (bottom).

Pléiades images

Consumer grade camera

5 Discussion and perspective

Avantage de la methode : modeles analyique, minimise deformation et residu, peut tre appliquee si on a que les points homologues (photo escalier ?).

Inconvenient ? Cas comme 7 pas gere, peut tre le sont il par Oh ?

Future work =¿ use MNT ? Test sur configuration plus compliques : orbites differentes ? Radar ? Radar/visible ?

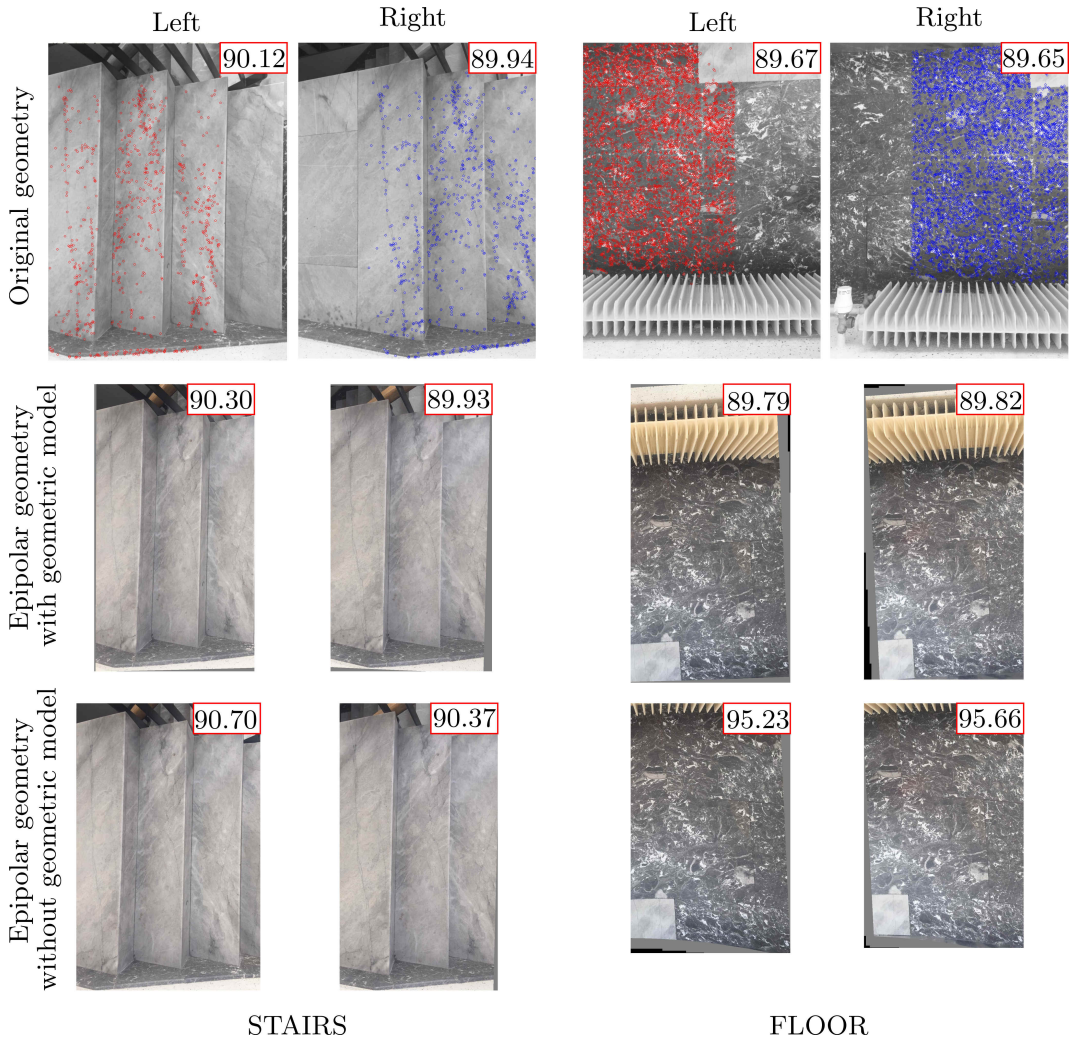

Figure 11: dddd consumer grade cam